1-7-2023

Pressure-induced charge orders and their postulated coupling to magnetism in hexagonal multiferroic $LuFe_2O_4$

Fengliang Liu

Yiqing Hao

Jinyang Ni

Yongsheng Zhao

Dongzhou Zhang

See next page for additional authors

Authors

Fengliang Liu, Yiqing Hao, Jinyang Ni, Yongsheng Zhao, Dongzhou Zhang, Gilberto Fabbris, Daniel Haskel, Shaobo Cheng, Xiaoshan Xu, Lifeng Yin, Hongjun Xiang, Jun Zhao, Xujie Lü, Wenbin Wang, Jian Shen, and Wenge Yang

ARTICLE OPEN

Check for updates

Pressure-induced charge orders and their postulated coupling to magnetism in hexagonal multiferroic $LuFe_2O_4$

Fengliang Liu[1,2,3,12], Yiqing Hao[1,12], Jinyang Ni[1,12], Yongsheng Zhao[2], Dongzhou Zhang[4], Gilberto Fabbris[5], Daniel Haskel[5], Shaobo Cheng[6], Xiaoshan Xu[7], Lifeng Yin[1,8,9,10,11], Hongjun Xiang[1,9], Jun Zhao[1,9,10], Xujie Lü[2], Wenbin Wang[8,9,10,11]✉, Jian Shen[1,8,9,10,11]✉ and Wenge Yang[2]✉

Hexagonal $LuFe_2O_4$ is a promising charge order (CO) driven multiferroic material with high charge and spin-ordering temperatures. The coexisting charge and spin orders on Fe^{3+}/Fe^{2+} sites result in magnetoelectric behaviors, but the coupling mechanism between the charge and spin orders remains elusive. Here, by tuning external pressure, we reveal three charge-ordered phases with suggested correlation to magnetic orders in $LuFe_2O_4$: (i) a centrosymmetric incommensurate three-dimensional CO with ferrimagnetism, (ii) a non-centrosymmetric incommensurate quasi-two-dimensional CO with ferrimagnetism, and (iii) a centrosymmetric commensurate CO with antiferromagnetism. Experimental in situ single-crystal X-ray diffraction and X-ray magnetic circular dichroism measurements combined with density functional theory calculations suggest that the charge density redistribution caused by pressure-induced compression in the frustrated double-layer [Fe_2O_4] cluster is responsible for the correlated spin-charge phase transitions. The pressure-enhanced effective Coulomb interactions among Fe-Fe bonds drive the frustrated (1/3, 1/3) CO to a less frustrated (1/4, 1/4) CO, which induces the ferrimagnetic to antiferromagnetic transition. Our results not only elucidate the coupling mechanism among charge, spin, and lattice degrees of freedom in $LuFe_2O_4$, but also provide a new way to tune the spin-charge orders in a highly controlled manner.

npj Quantum Materials (2023)8:1 ; https://doi.org/10.1038/s41535-022-00522-x

INTRODUCTION

Multiferroic materials have attracted lots of research interests during the last decades because of their great potential applications in electronic devices and spintronics[1,2]. Hexagonal $LuFe_2O_4$ is a promising candidate material for charge order (CO) driven multiferroicity, which has been intensively investigated both from fundamental and applied perspectives[3–10]. Previous X-ray diffraction (XRD)[4] and transmission electron microscopy (TEM) measurements[11,12] have suggested that $LuFe_2O_4$ exhibits three-dimensional (3D) CO at ambient pressure, manifesting a periodic arrangement of low-valence (Fe^{2+}) and high-valence (Fe^{3+}) ions. Possible evidence for CO-driven ferroelectricity of $LuFe_2O_4$ was also reported[3,13,14], although its origin remains debated[15]. In addition to the 3D order of Fe^{2+}-Fe^{3+} ions observed below the CO transition temperature T_{CO} (~320 K), a quasi-2D (Q2D) ordering of Fe^{2+}-Fe^{3+} was also observed above T_{CO} persisting up to ~525 K[12]. Furthermore, neutron diffraction measurements have revealed the ferrimagnetic order of Fe moments below the Neel transition temperature T_N (~240 K)[16]. It is therefore suggested that the correlations between charge and magnetic order associated with Fe^{2+} and Fe^{3+} ions may play a crucial role in the multiferroicity in $LuFe_2O_4$[4,17–20].

Application of external pressure is a powerful and clean tool to gain deep insights into the interplay between the charge, magnetic and structural degrees of freedom, because the strong frustration involved in the spin and charge orders in the triangular lattice of $LuFe_2O_4$ may result in high tunable ground states[17,20]. However, high-pressure diffraction measurements are often difficult owing to the reduced beam flux and increased background caused by pressure cells. Previous neutron diffraction measurements on powder samples of $LuFe_2O_4$ revealed a ~30% reduction of the ferrimagnetic ordered-moments up to ~3 GPa[21], and X-ray powder diffraction showed indications for pressure-induced structural phase transitions[22]. However, the positions and intensities of superlattice reflections observed in powder diffraction showed non-systematic evolution with increasing pressure, probably due to poor powder averaging, thus preventing an accurate description of the pressure-induced phases[22]. Moreover, neutron and X-ray powder diffraction measurements have revealed a high-pressure polymorph phase $LuFe_2O_4$-*hp*[23,24] above 12 GPa. The $LuFe_2O_4$-*hp* phase retained its structure after pressure release, thus allowing ex-situ measurement at ambient pressure[23,24]. This $LuFe_2O_4$-*hp* phase adopts a rectangular Fe lattice[24] and is not directly relevant to the frustrated triangular lattice of $LuFe_2O_4$ at ambient conditions. Therefore, despite the intensive efforts, the pressure-dependent evolution of the frustrated charge and magnetic interactions in the multiferroic $LuFe_2O_4$ remains unclear.

Here, we investigated the evolution of charge orders under pressure and the accompanied spin orders in $LuFe_2O_4$ using the in situ high-pressure single-crystal X-ray diffraction (HP-SXD) and high-pressure X-ray magnetic circular dichroism (HP-XMCD)

[1]State Key Laboratory of Surface Physics and Department of Physics, Fudan University, Shanghai 200433, China. [2]Center for High Pressure Science and Technology Advanced Research (HPSTAR), Shanghai 201203, China. [3]Department of Physics, Nanchang University, Nanchang 330031, China. [4]Hawaii Institute of Geophysics & Planetology, University of Hawaii Manoa, Honolulu, HI, USA. [5]Advanced Photon Source, Argonne National Laboratory, Argonne, IL 60439, USA. [6]Department of Condensed Matter Physics and Materials Science, Brookhaven National Laboratory, Upton, NY 11973, USA. [7]Department of Physics and Astronomy, University of Nebraska, Lincoln, NE 68588, USA. [8]Institute for Nanoelectronic Devices and Quantum Computing, Fudan University, Shanghai 200433, China. [9]Collaborative Innovation Center of Advanced Microstructures, Nanjing 210093, China. [10]Shanghai Qi Zhi Institute, Shanghai 200232, China. [11]Shanghai Research Center for Quantum Sciences, Shanghai 201315, China. [12]These authors contributed equally: Fengliang Liu, Yiqing Hao, Jinyang Ni. ✉email: wangwb@fudan.edu.cn; shenj5494@fudan.edu.cn; yangwg@hpstar.ac.cn

spectroscopy. A series of pressure-induced charge order phases, including a Q2D CO phase below 5.5 GPa and a 3D CO phase at higher pressure (6.0–12.6 GPa), were identified by HP-SXD measurements. In addition, the HP-XMCD measurements suggest that the Q2D and 3D CO phases are associated with non-zero and zero net magnetization, respectively, which is interpreted as indicative of ferrimagnetic and antiferromagnetic orders. The pressure-induced charge- and magnetic-order phase transitions can be further interpreted by density functional theory (DFT) calculations. These results suggest that the CO phases are intimately coupled with magnetism, both of which can be manipulated by external pressure in a highly controlled manner in hexagonal layered multiferroic $LuFe_2O_4$.

RESULTS

Crystal structure and SXD diffraction patterns

$LuFe_2O_4$ adopts a bi-layered triangular lattice structure with space group *R*-3*m* (No. 166) at ambient pressure. Considering the CO and the atomic displacement it induces, the trigonal lattice splits into three 120° twinned monoclinic lattices, each of which adopts the space group *C*2/*m* (No.12). The transformation between the trigonal and monoclinic lattices is shown in Fig. 1a. The optimal stoichiometry of our sample was confirmed by magnetic susceptibility and transmission electron microscopes measurements at ambient pressure (See Supplementary Fig. 1 and Note 1). Our high-pressure synchrotron X-ray diffraction measurement of $LuFe_2O_4$ (See Supplementary Methods and Supplementary Fig. 2) was carried out on a high-quality single-crystalline sample. Within the representation of space group *C*2/*m* (See details in Supplementary Fig. 3 and Note 3), the lattice parameters are $a = 5.957(2)$ Å, $b = 3.434(4)$ Å, $c = 8.642(3)$ Å, and $\beta = 103.28(2)^\circ$ at 300 K and 0.8 GPa. The lattice parameters *a*, *b*, and *c* shrink with increasing pressure. At 300 K and 12.6 GPa, the lattice parameters become $a = 5.809(5)$ Å, $b = 3.339(16)$ Å, $c = 8.374(11)$ Å, and $\beta = 103.39(9)^\circ$ with a volume reduction of 8.2(6)%.

Charge order phase transition under pressure

Apart from the lattice shrinkage, a series of superlattice peaks were also observed with a wave vector $\boldsymbol{k}_{AP} = (1/3, 1/3, 3/2)_T$ in trigonal lattice or $(0, 2/3, 1/2)_M$ in the monoclinic lattice at 0.8 GPa, as illustrated in Fig. 1b and Fig. 1f. This wave vector is close to that observed at ambient pressure where the charge order of low-valence (Fe^{2+}) and high-valence (Fe^{3+}) Fe ions forms a $\sqrt{3}\times\sqrt{3}\times 2$ superlattice[4] (Fig. 2b). As pressure further increases, the superlattice peaks exhibit drastic broadening along the *L*-direction (Fig.1b–d), indicating that the charge order becomes quasi-two-dimensional. Meanwhile, the maximum peak intensity in the L-direction moves from half-integer ($L = n + 1/2$) at ambient pressure to integer ($L = n$) at 5.0 GPa (see Fig. 1d–g and details in Supplementary Fig. 4 and Note 4), indicating that the inter-plane polarization emerges under pressure (Fig. 2d). Interestingly, similar quasi-two-dimensional charge order was also observed above the 3D charge ordering temperature of 320 K in $LuFe_2O_4$ at ambient pressure[4].

A closer inspection of the diffraction pattern actually reveals a tiny incommensurability of the charge order wave vector [$\boldsymbol{k}_{AP} = (1/3+\delta, 1/3+\delta, 3/2)_T$ and $\boldsymbol{k}_{2D} = (1/3-\delta, 1/3-\delta, 0)_T$] at 0.8 GPa. The incommensurability increases dramatically with increasing pressure and eventually reaches a commensurate position $\boldsymbol{k}_{HP} = (1/4, 1/4, 0)_T$ at pressures above 6.0 GPa. In contrast to the broadened diffraction patterns along the *L*-direction for the superstructure below 5.0 GPa (Fig. 1d), the $(1/4, 1/4, 0)_T$ phase shows sharp peak features both along the in-plane (*HK*) and out-of-plane (*L*) directions (Fig. 1e, h), indicating restoration of robust 3D order. Meanwhile, the sharpening of the emerging $(1/4, 1/4, 0)_T$ peak in the 3D CO phase also rules out the possibility of non-hydrostaticity as the reason why the intermediate quasi-2D CO phase shows a broadening of peaks along L-directions. This commensurate 3D CO-HP phase persists up to 12.6 GPa without a major change in the primary structure. Interestingly, the pressure dependence of resistivity also shows a kink feature at around 6 GPa, indicative of the (1/3, 1/3) to (1/4, 1/4) phase transition (see Supplementary Fig. 5 and Note 5).

The evolution of the incommensurability of the superlattice peaks in the HK-plane under various pressures is summarized in Fig. 1i. There are three 120-degree twinned charge orders in $LuFe_2O_4$, each with a unique ***k***-vector, therefore the superlattice peak position differs for each charge order twin, forming a spiral-like diffraction pattern in reciprocal space. As pressure increases, the centers of charge order peaks move away from (1/3, 1/3) along the 120-degree directions in the *HK*-plane and eventually reach (1/4, 1/4), (1/2, 1/4), (1/4, 1/2) at 6.0 GPa. Therefore, the quasi-2D charge order phase observed in the 3.1 to 5.0 GPa range can be regarded as an intermediate phase between the commensurate (1/3, 1/3) and (1/4, 1/4) charge order phases.

We now discuss the possible charge order models for the high-pressure phases. We consider two valence states of Fe ions (Fe^{2+} and Fe^{3+}). Based on diffraction data, we found that the charge order of $(1/4, 1/4, 0)_T$ phase can be best described with the P_b2/c (BNS 13.71) black-white space group (see Fig. 2e–f and details in Supplementary Fig. 6, Table 1, and Note 6). The CO phase models of CO-AP [$\boldsymbol{k}_{AP} = (1/3, 1/3, 3/2)_T$], CO-2D [$\boldsymbol{k}_{2D} = (1/3, 1/3, 0)_T$], and CO-HP [$\boldsymbol{k}_{HP} = (1/4, 1/4, 0)_T$] are illustrated in Fig. 2a–f, respectively. These CO models are further supported by DFT calculation (Fig. 4d). The evolution from $(1/3, 1/3)_T$ to $(1/4, 1/4)_T$ can be understood through the Coulomb interactions on different types of Fe-Fe bonds. In CO-AP and CO-2D phases, 5/9 of the nearest-neighbor (NN), 2/3 of the second NN, and 5/9 of the third NN Fe bonds are Fe^{2+}-Fe^{3+} bonds. On the contrary, in the CO-HP phase, 2/3 of the NN, 2/3 of the second NN, and 1/3 of the third NN Fe bonds are Fe^{2+}-Fe^{3+} bonds. The above observation provides a natural understanding, that the effective Coulomb interactions of NN and third NN Fe-Fe pairs are tuned by the compression in frustrated triangular double-layer Fe_2O_4 structure due to increased pressure. We also calculated the interlayer next-nearest-neighbor (V_{cNNN}) and intralayer nearest-neighbor (V_{abNN}) Coulomb interactions at each pressure point. Our result shows that V_{cNNN}/V_{abNN} remains almost unchanged in the region of 1 to 5 GPa, and drops sharply above 6 GPa where the $(1/4, 1/4)_T$ CO phase is favored[25] (see Supplementary Fig. 7 and Note 7). We note that the observed high pressure (1/4, 1/4, 0) CO in $LuFe_2O_4$ is different from the (1/4, 1/4) CO phase revealed by transmission electron microscopy in YFe_2O_4 at ambient pressure[26]. Later X-ray diffraction experiments suggested that this CO phase is actually characterized by (1/4, 1/2, 1/4) with a triclinic supercell four times larger along the *c*-axis[27].

Magnetic phase transition under pressure

In order to inform on the magnetic ground states associated with these charge-ordered phases, we utilized HP-XMCD spectroscopy to monitor the change of net magnetization of $LuFe_2O_4$ under pressure. Figure 3a shows Fe K-edge isotropic absorption (XAS) and dichroic (XMCD) signals in $LuFe_2O_4$ at 100 K and 5 T. The measurements were performed at the Fe *K*-edge instead of the more commonly used Fe *L*-edge because soft X-ray MCD is incompatible with the highly absorbing diamond anvil cell environment[28–30]. The dichroic signal at 1.9 GPa consists of a positive peak in the pre-edge region (7114.0 eV) and another positive peak near the main rising edge peak (7129.0 eV) with larger intensity (Fig. 3a). With increasing pressure, these two dichroic peaks become weaker at 4.3 GPa, and these two peaks are not observed at the higher pressure of 9.5 GPa. The peaks of Fe *K*-edge XAS and XMCD signals observed at 1.9 GPa are in

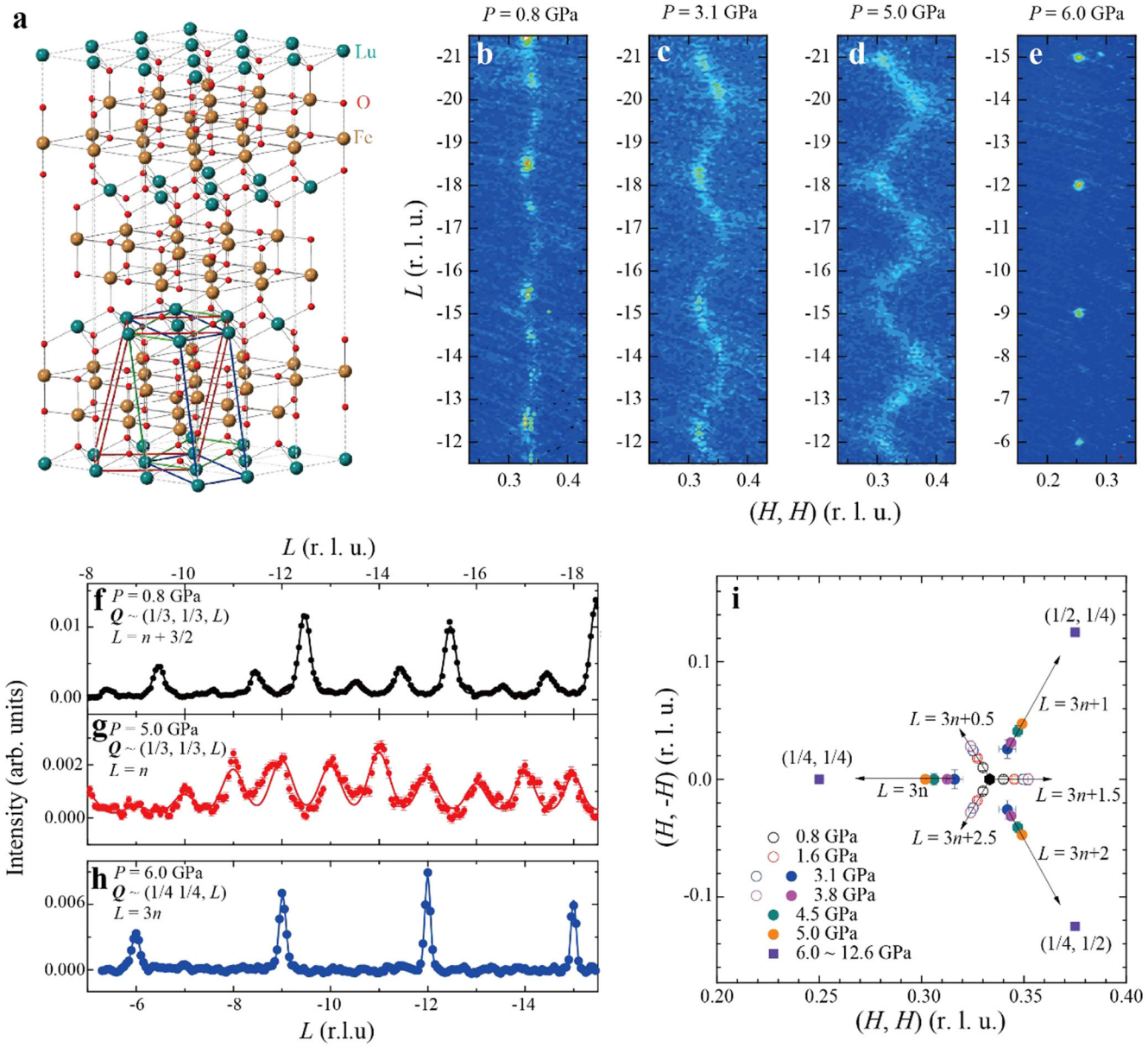

Fig. 1 Crystal structure and charge order evolution of $LuFe_2O_4$ under high pressure at room temperature. a Crystal structure of $LuFe_2O_4$ at ambient pressure. Dotted lines represent the trigonal lattices. Red, blue, and green solid lines represent three equivalent monoclinic lattices with different twinned directions. **b**–**e** Single-crystal X-ray diffraction (SXD) intensities in the (*HHL*) scattering plane measured near the charge ordering (CO) superlattice peaks at room temperature at 0.8, 3.1, 5.0, and 6.0 GPa, respectively. **f**–**h** SXD intensity along the $\boldsymbol{Q} = (1/3, 1/3, L)$, (1/3, 1/3, *L*), and (1/4, 1/4, *L*) direction measured at 0.8, 5.0, and 6.0 GPa, respectively. The Solid lines in Fig. 1f–h are fittings using Gaussian peaks. **i** Summary of the charge order peak positions in *HK*-plane measured from 0.8 to 12.6 GPa. The black hexagon in the center indicates (*H*, *H*) = (1/3, 1/3).

agreement with those observed at ambient pressure (see Supplementary Fig. 8 and Note 8)[31]. Therefore, the magnetic order at 1.9 GPa is best interpreted as a ferrimagnetic structure which was unveiled by the previous L-edge XMCD[19] and neutron diffraction[16] measurements at ambient pressure. The weaker XMCD signals observed at 4.3 GPa indicate reduced net magnetization compared to 1.9 GPa. In previous high-pressure neutron powder diffraction measurements, it is shown that the ferrimagnetic order of $LuFe_2O_4$ is preserved below 3 GPa while the ordered-moments gradually reduced from 4.5 μ_B/Fe to 3 μ_B/Fe[21]. Therefore, the proportionally reduced XMCD signal at 4.3 GPa is best interpreted by the same ferrimagnetic structure and further reduced magnetic ordered-moments, which could be related to pressure-induced magnetic disorders. The zero XMCD signal at 9.5 GPa indicates zero net magnetization, suggesting an antiferromagnetic ground state in the HP-CO phase, which is further discussed in the DFT calculation results. Insets of Fig. 3a–c illustrate the pre-edge region of XAS and XMCD signals. The positions of the XAS pre-edge peak and leading edge do not shift by pressure, which indicates that the valence ratio of Fe^{2+} and Fe^{3+} remains unchanged (see Supplementary Fig. 9), in agreement with the CO models illustrated in Fig. 2.

DISCUSSION

More insight into the nature of the magnetic ground states associated with the CO phases in pressurized $LuFe_2O_4$ can be also obtained by DFT calculations. For the CO-AP phase and CO-2D

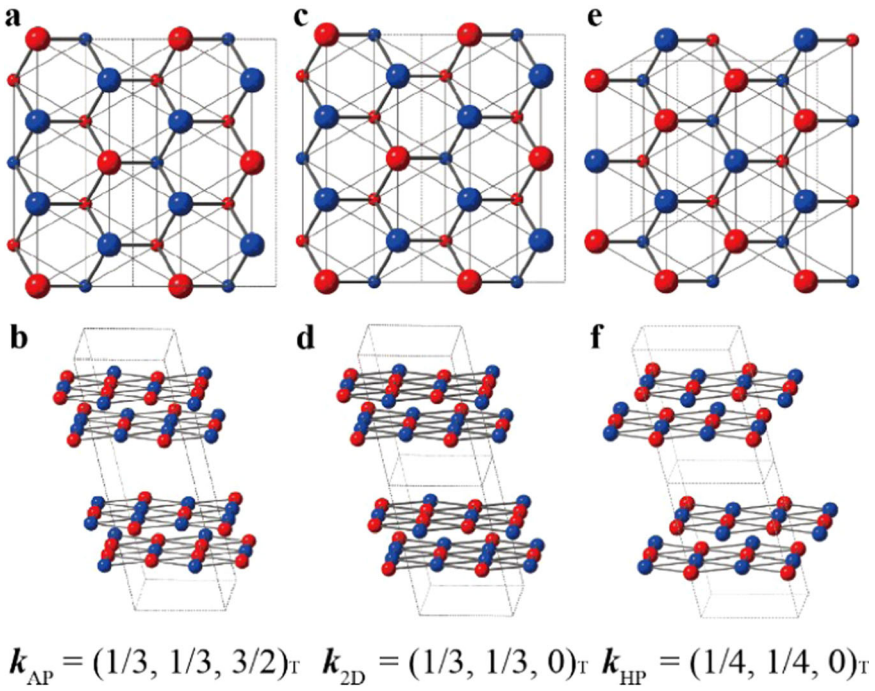

Fig. 2 Charge order models of $LuFe_2O_4$ corresponding to observed SXD pattern from 0.8 to 12.6 GPa. Red and blue spheres represent Fe^{2+} and Fe^{3+} ions, respectively. Sphere size in (**a**, **c**, **e**) indicates the Fe ions in different planes. Thick and thin solid lines represent the nearest neighbored (NN) and next-nearest neighbored (NNN) Fe-Fe pairs, respectively. Dashed lines represent lattice boundaries. **a**, **b** Centrosymmetric CO-AP model with $\boldsymbol{k} \sim (1/3, 1/3, 3/2)$. **c**, **d** Non-centrosymmetric CO-2D model with $\boldsymbol{k} \sim (1/3, 1/3, 0)$ at $P = 5.0$ GPa. Noted the interlayer arrangements in (**b**) and (**d**) are different due to changes in the L-component of the wave vector. **e**, **f** CO-HP model for $\boldsymbol{k} = (1/4, 1/4, 0)$, corresponding SXD patterns observed between 6.0 and 12.6 GPa.

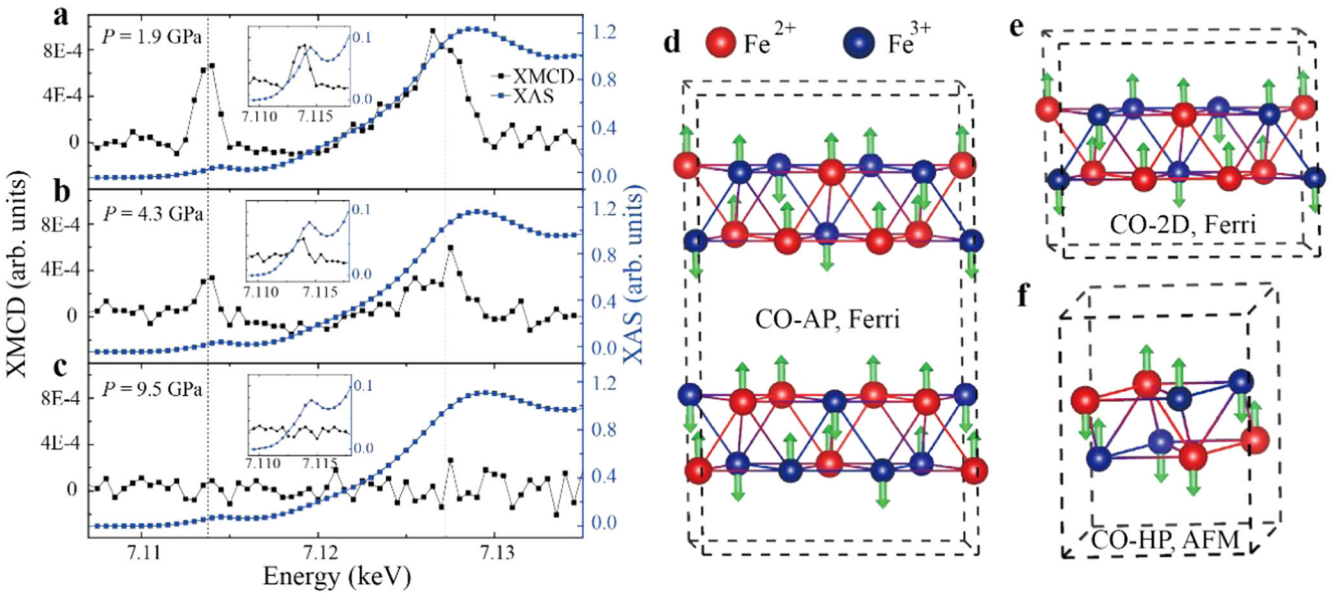

Fig. 3 Magnetic properties of $LuFe_2O_4$ under pressure. a–c Fe K-edge X-ray absorption near edge structure (XAS) and XMCD spectroscopy data measured at $T = 100$ K, $H = 5$ T, and $P = 1.9$ GPa (**a**), 4.3 GPa (**b**), 9.5 GPa (**c**), respectively. The pressures correspond to the three observed charge order phases (CO-AP, CO-2D, CO-HP) in $LuFe_2O_4$. Insets of (**a**–**c**) show the XAS and XMCD data of the pre-edge region at 1.9, 4.3, and 9.5 GPa, respectively. **d** Ferrimagnetic model for the centrosymmetric CO-AP phase **e** Ferrimagnetic model for the non-centrosymmetric CO-2D phase **f** Antiferromagnetic model for the centrosymmetric CO-HP phase for DFT calculations in pressurized $LuFe_2O_4$. (Ferri (ferrimagnetic), AFM (antiferromagnetic)).

phase, DFT calculations show that $LuFe_2O_4$ adopts the "2:1 ferrimagnetic state" as the ground state. In this state, as shown in Fig. 3d, e, the majority spin orientation consists of all Fe^{2+} ions plus one-third of total Fe^{3+} ions, while the minority spin orientation consists of the remaining Fe^{3+} ions. DFT calculation shows that the antiferromagnetic structure in Fig. 3f is the preferred magnetic ground state for the CO-HP phase (see Supplementary Fig. 10). In this state, both Fe^{2+} and Fe^{3+} are evenly separated in opposite spin orientations, resulting in the centrosymmetric electromagnetic order, and thus leading to a

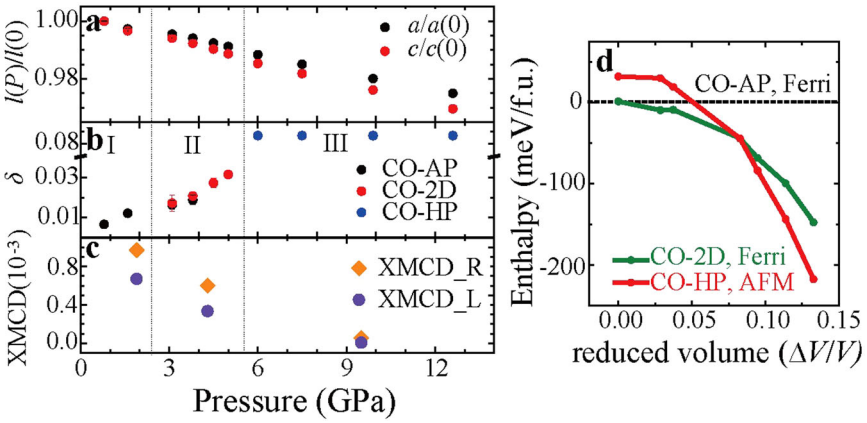

Fig. 4 Phase diagram of $LuFe_2O_4$ under pressure. a Relative reduction of lattice parameters *a* and *c* by increased pressure measured between 0.8 and 12.6 GPa. **b** Evolution of in-plane incommensurate CO wave vector δ by pressure. δ is defined by $(1/3+\delta, 1/3+\delta)$ in CO-AP and $(1/3-\delta, 1/3-\delta)$ in CO-2D. The commensurate CO wave vector (1/4, 1/4) of CO-HP is represented by $\delta = 1/12$. **c** The pressure dependence of XMCD spectral weight. **d** The pressure dependence of relative enthalpies between the charge order phases mentioned in Figs. 2 and 3d–f. (ferri (ferrimagnetic), AFM (antiferromagnetic)).

zero net magnetic moment in this phase. Therefore, this DFT calculation result is consistent with the XMCD measurement, showing that the net magnetization of frustrated $LuFe_2O_4$ is completely suppressed at 9.5 GPa in the CO-HP phase.

Combining the HP-SXD, HP-XMCD, and DFT calculations, we have found a series of 3D-2D-3D charge order transitions in the hexagonal $LuFe_2O_4$. The emergence of the CO-HP phase at high pressure appears to be accompanied by a ferrimagnetic to antiferromagnetic transition (Fig. 3d–f). We calculate the pressure dependence of the enthalpy for each spin-charge-ordered phase using GGA + *U* method[32,33], as illustrated in Fig. 4d. According to the calculation, at ambient pressure, the 3D centrosymmetric CO phase (CO-AP) combined with 2:1 ferrimagnetic order (Fig. 3d) is most favored. Then, as the lattice shrinks with applying hydrostatic pressure (Fig. 4a), a 2D non-centrosymmetric CO phase (CO-2D) with 2:1 ferrimagnetic order (Fig. 3e) becomes the ground state. At higher pressure, a 3D centrosymmetric CO phase (CO-HP) with antiferromagnetic order (Fig. 3f) becomes the ground state. During the CO-AP to CO-2D phase transition, the Fe-Fe bonds within the $[Fe_2O_4]$ bilayer structure are compressed by pressure. Such compression enhanced the Coulomb interaction among bilayer Fe-Fe bonds, thus enhancing the hopping matrix elements between low-valence and high-valence Fe sites in the frustrated lattice, which could result in damping of out-of-plane correlations and incommensurability in ab-plane (Fig. 1b–d). As the pressure further increases, the effective Coulomb interaction among Fe-Fe bonds reaches a critical point where the $Q = (1/3, 1/3)$ charge orders cannot be sustained. Thus the system evolves into a less frustrated $Q = (1/4, 1/4)$ CO-HP charge order where all Fe layers are charge neutral. Due to the suggested strong coupling between charge and spin correlations, such drastic redistribution of charge density, in turn, causes a substantial change in the magnitude of spin–spin interactions. As a result, the magnetic moments on Fe^{2+} and Fe^{3+} are re-arranged and the magnetic structure evolves from ferrimagnetism to antiferromagnetic order. The DFT calculations and experimental evidence indicate that the observed charge ordering and magnetic transitions are coupled and strongly correlated with the compression of the crystalline lattice.

In summary, we have conducted a systematic study on the evolution of the crystal structure and charge orders and their accompanied spin orders in hexagonal $LuFe_2O_4$ under pressure using the in situ HP-SXD and HP-XMCD measurements. With increasing pressure, the system exhibits three correlated charge-ordered ground states: (1) the centrosymmetric 3D CO-AP phase with ferrimagnetic order, (2) the non-centrosymmetric CO-2D phase with ferrimagnetic order, and (3) the centrosymmetric 3D CO-HP phase with antiferromagnetic order. These results suggest a strong coupling between charge and magnetic orders in hexagonal $LuFe_2O_4$. The evolution of the charge and magnetic order under pressure is further supported by the DFT calculations, which show that the phase transitions are the result of tuned frustrated charge and spin interactions induced by the compression of triangular Fe_2O_4 double-layer structures. Our results provide important insights on realizing the potential charge order induced multiferroicity in $LuFe_2O_4$, and also suggest that hydrostatic pressure is a powerful tool to unveil charge and magnetic order states in similar systems such as RFe_2O_4 (R = Y, Yb…), where competition between different types of charge orders has been already observed at ambient pressure[26,27,34–36]. It is, therefore, particularly interesting to investigate if similar ferroelectric (1/3, 1/3, 0) CO or (1/4, 1/4, 0) CO could be achieved in RFe_2O_4 materials through applying external pressure or chemical doping.

METHODS

Sample preparation

Single crystals of $LuFe_2O_4$ were grown by the floating-zone method using a CO/CO_2 (~2.7:1) mixed atmosphere to control oxygen stoichiometry. Our electron probe micro analyzer (EPMA) measurement on the single-crystalline sample shows almost optimal stoichiometry of $Lu_{1.01(1)}Fe_2O_{3.97(4)}$.

High-pressure measurement

Single-crystal X-ray diffraction (SXD) experiment was conducted at synchrotron radiation beamline 13BM-C, Advanced Photon Source (APS), Argonne National Lab (ANL), using monochromatic X-rays with 0.434 Å wavelength, with the pressure increasing from 0.8 GPa up to 14.5 GPa. The 1-deg step scan, wide-step scan, and whole-range scan were performed with a scanning angle range of ±35 degrees at each pressure point[37]. Symmetry analysis was conducted using Sarah software[38] and Bilbao Crystallographic Server[39], and structure refinements were conducted using FULL-PROF program suite[40]. High-pressure synchrotron X-ray Magnetic Circular Dichroism (XMCD) spectroscopy measurements with the energy scanning across the Fe K-edge were conducted at beamline 4ID-D, APS, and ANL. Circularly polarized X-rays were generated with a diamond phase retarder. To obtain the XMCD

signal, the X-ray helicity was modulated at 13.1 Hz, and XMCD signals were detected with a phase lock-in amplifier. In addition, XMCD scans were repeated with opposite applied field direction to ensure artifact-free XMCD signals[41]. Corresponding to the three observed CO phases in pressurized $LuFe_2O_4$, the XMCD data were collected at 1.9, 4.3, and 9.5 GPa. In these measurements, a magnetic field was set to +5T/−5T and the temperature to 100 K. X-ray Absorption Spectroscopy (XAS) data is collected simultaneously during the XMCD measurement and obtained by averaging X-ray absorption for opposite X-ray helicities. The pressure was determined by the in situ ruby fluorescence measurement system[42] with a pressure uncertainty of less than 5%. An offline ruby system was used in the SXD measurement, before and after each manual pressure change at ambient temperature. For the low-temperature XMCD measurements, online membrane and ruby fluorescence systems were used to apply and measure pressure, respectively (See details in supplementary Methods).

Density functional theory (DFT) calculations

The first-principle density functional theory calculations are based on the projector augmented wave (PAW) method[43] encoded in the Vienna ab initio simulation package (VASP)[44]. The exchange-correlation functional of the Perdew–Becke–Erzenh (PBE)[45] form is adopted and the plane-wave cutoff energy is set to 500 eV. To properly describe the strong electron correlation in the Fe 3*d* states, the GGA plus on-site repulsion *U* method (GGA + *U*)[32] was employed with the effective *U* value ($U_{eff} = U - J$) of 4 eV. Calculations with various U_{eff} show that the main results remain valid when U_{eff} is varied between ~3.1 and 5.5 eV. The structural optimizations are carried out until the forces acting on atoms are smaller than 0.01 eVÅ^{-1}. To obtain the energy of each charge order structure, GGA + *U* calculations were carried out in two steps[33]. For each charge order structure, we first optimize the chosen charge order structure using a large *U* (e.g., $U_{eff} = 7.5$ eV). Then we re-optimize the charge order structure with a smaller *U* (i.e., $U_{eff} = 4$ eV) using the converged charge densities obtained with the large *U*. It is noted that a larger U_{eff} was employed only to generate an initial charge density with the desired charge order structure. The enthalpies of each charge order phase under various pressure are calculated by the following expression: $H = U - PV$, where *H* is enthalpy, *U* is total energy, and *PV* is the product of pressure and volume. For each CO phase, atomic positions were relaxed while the lattice constants are constrained at the experimental values (see Fig. 4a and Supplementary Fig. 11).

DATA AVAILABILITY

The data supporting this study are available from the corresponding author upon reasonable request.

Received: 9 December 2021; Accepted: 7 November 2022;
Published online: 07 January 2023

REFERENCES

1. Fiebig, M., Lottermoser, T., Meier, D. & Trassin, M. The evolution of multiferroics. *Nat. Rev. Mater.* **1**, 1–14 (2016).
2. Spaldin, N. A. & Ramesh, R. Advances in magnetoelectric multiferroics. *Nat. Mater.* **18**, 203–212 (2019).
3. Ikeda, N. et al. Ferroelectricity from iron valence ordering in the charge-frustrated system $LuFe_2O_4$. *Nature* **436**, 1136–1138 (2005).
4. Angst, M. et al. Charge order in $LuFe_2O_4$: antiferroelectric ground state and coupling to magnetism. *Phys. Rev. Lett.* **101**, 227601 (2008).
5. Hervieu, M. et al. Oxygen storage capacity and structural flexibility of $LuFe_2O_{4+x}$ (0 < =x < =0.5). *Nat. Mater.* **13**, 74–80 (2014).
6. Mundy, J. A. et al. Atomically engineered ferroic layers yield a room-temperature magnetoelectric multiferroic. *Nature* **537**, 523–527 (2016).
7. Zhang, Y. et al. Effect of oxygen interstitial ordering on multiple order parameters in rare earth ferrite. *Phys. Rev. Lett.* **123**, 247601 (2019).
8. Deng, S. et al. Charge-lattice coupling in hole-doped $LuFe_2O_{4+\delta}$: the origin of second-order modulation. *Phys. Rev. Lett.* **122**, 126401 (2019).
9. Bourgeois, J. et al. Evidence of magnetic phase separation in $LuFe_2O_4$. *Phys. Rev. B* **86**, 024413 (2012).
10. Wang, W. et al. Growth diagram and magnetic properties of hexagonal $LuFe_2O_4$ thin films. *Phys. Rev. B* **85**, 155411 (2012).
11. Zhang, Y., Yang, H. X., Ma, C., Tian, H. F. & Li, J. Q. Charge-stripe order in the electronic ferroelectric $LuFe_2O_4$. *Phys. Rev. Lett.* **98**, 247602 (2007).
12. Zhang, Y. et al. Structure, charge ordering and physical properties of $LuFe_2O_4$. *Phys. Rev. B* **76**, 184105 (2007).
13. Subramanian, M. A. et al. Giant room-temperature magnetodielectric response in the electronic ferroelectric $LuFe_2O_4$. *Adv. Mater.* **18**, 1737–1739 (2006).
14. Yoshii, K., Ikeda, N., Matsuo, Y., Horibe, Y. & Mori, S. Magnetic and dielectric properties of RFe_2O_4, $RFeMO_4$, and $RGaCuO_4$ (R = Yb and Lu, M = Co and Cu). *Phys. Rev. B* **76**, 024423 (2007).
15. de Groot, J. et al. Charge order in $LuFe_2O_4$: an unlikely route to ferroelectricity. *Phys. Rev. Lett.* **108**, 187601 (2012).
16. Christianson, A. D. et al. Three-dimensional magnetic correlations in multiferroic $LuFe_2O_4$. *Phys. Rev. Lett.* **100**, 107601 (2008).
17. Xu, X. S. et al. Charge order, dynamics, and magnetostructural transition in multiferroic $LuFe_2O_4$. *Phys. Rev. Lett.* **101**, 227602 (2008).
18. Ko, K. T. et al. Electronic origin of giant magnetic anisotropy in multiferroic $LuFe_2O_4$. *Phys. Rev. Lett.* **103**, 207202 (2009).
19. Kuepper, K. et al. Charge order, enhanced orbital moment, and absence of magnetic frustration in layered multiferroic $LuFe_2O_4$. *Phys. Rev. B* **80**, 220409 (2009).
20. Mulders, A. M. et al. Direct observation of charge order and an orbital glass state in multiferroic $LuFe_2O_4$. *Phys. Rev. Lett.* **103**, 077602 (2009).
21. Makarova, O. L. et al. Pressure effect on the magnetic order of $LuFe_2O_4$. *Appl. Phys. Lett.* **103**, 082907 (2013).
22. Poienar, M. et al. P-T phase diagram of $LuFe_2O_4$. *Crystals* **8**, 184 (2018).
23. Rouquette, J. et al. Pressure-induced structural transition in $LuFe_2O_4$: towards a new charge ordered state. *Phys. Rev. Lett.* **105**, 237203 (2010).
24. Damay, F. et al. High-pressure polymorph of $LuFe_2O_4$ with room-temperature antiferromagnetic order. *Phys. Rev. B* **91**, 214111 (2015).
25. Nagano, A., Naka, M., Nasu, J. & Ishihara, S. Electric polarization, magnetoelectric effect, and orbital state of a layered iron oxide with frustrated geometry. *Phys. Rev. Lett.* **99**, 217202 (2007).
26. Ikeda, N., Mori, R., Mori, S. & Kohn, K. Structure transition and charge competition on YFe_2O_4. *Ferroelectrics* **286**, 175–184 (2011).
27. Blasco, J. et al. Characterization of competing distortions in YFe_2O_4. *Phys. Rev. B* **93**, 184110 (2016).
28. Letard, I., Sainctavit, P. & Deudon, C. XMCD at Fe $L_{2,3}$ edges, Fe and S K-edges on Fe_7S_8. *Phys. Chem. Miner.* **34**, 113–120 (2006).
29. Mathon, O. et al. XMCD under pressure at the Fe K-edge on the energy-dispersive beamline of the ESRF. *J. Synchrotron Radiat.* **11**, 423–427 (2004).
30. Haskel, D., Tseng, Y. C., Lang, J. C. & Sinogeikin, S. Instrument for x-ray magnetic circular dichroism measurements at high pressures. *Rev. Sci. Instrum.* **78**, 083904 (2007).
31. Lafuerza, S. et al. Electronic states of RFe_2O_4 (R = Lu,Yb,Tm,Y) mixed-valence compounds determined by soft x-ray absorption spectroscopy and x-ray magnetic circular dichroism. *Phys. Rev. B* **90**, 245137 (2014).
32. Liechtenstein, A. I., Anisimov, V. V. & Zaanen, J. Density-functional theory and strong interactions: Orbital ordering in Mott-Hubbard insulators. *Phys. Rev. B Condens Matter* **52**, R5467–R5470 (1995).
33. Xiang, H. J. & Whangbo, M. H. Charge order and the origin of giant magnetocapacitance in LuFe2O4. *Phys. Rev. Lett.* **98**, 246403 (2007).
34. Nagata, T. & Ikeda, N. Modulation in charge ordering structure of ferroelectric $YbFe_2O_4$ by magnetic ordering. *AIP Adv.* **8**, 075312 (2018).
35. Horibe, Y. et al. Crystallographical and morphological changes in charge-ordering transition of RFe_2O_4 (R: Y, Lu) investigated by transmission electron microscopy. *Ferroelectrics* **584**, 20–30 (2021).
36. Horibe, Y., Yoshii, K., Ikeda, N. & Mori, S. Oxygen-deficient effect on charge ordering in spin- and charge- frustrated ferrite $YFe_2O_{4-\delta}$. *Phys. Rev. B* **80**, 092104 (2009).
37. Zhang, D. et al. High pressure single crystal diffraction at PX^2. *J. Vis. Exp.* e54660 (2017).
38. Wills, A. S. A new protocol for the determination of magnetic structures using simulated annealing and representational analysis (SARAh). *Phys. B Condens. Matter* **276**, 680–681 (2000).

39. Aroyo, M. I. et al. Crystallography online: Bilbao crystallographic server. *Bulg. Chem. Commun.* **43**, 183–197 (2011).
40. Rodríguez-Carvajal, J. Recent advances in magnetic structure determination by neutron powder diffraction. *Physica. B Condens. Matter* **192**, 55–69 (1993).
41. Sun, F. et al. Pressure effect on the magnetism of the diluted magnetic semiconductor $(Ba_{1-x}K_x)(Zn_{1-y}Mn_y)_2As_2$ with independent spin and charge doping. *Phys. Rev. B* **93**, 224403 (2016).
42. Piermarini, G. J., Block, S., Barnett, J. D. & Forman, R. A. Calibration of the pressure dependence of the R1 ruby fluorescence line to 195 kbar. *J. Appl. Phys.* **46**, 2774–2780 (1975).
43. Blochl, P. E. Projector augmented-wave method. *Phys. Rev. B Condens Matter* **50**, 17953–17979 (1994).
44. Kresse, G. & Furthmuller, J. Efficient iterative schemes for ab initio total-energy calculations using a plane-wave basis set. *Phys. Rev. B Condens Matter* **54**, 11169–11186 (1996).
45. Perdew, J. P., Burke, K. & Ernzerhof, M. Generalized gradient approximation made simple. *Phys. Rev. Lett.* **77**, 3865–3868 (1996).

ACKNOWLEDGEMENTS

This work was supported by the National Natural Science Foundation of China (Grant Nos. U1930401, 12074071, 51772184, and 11991060) and the National Key Research Program of China (2016YFA0300702). We acknowledge Dr. Lili Zhang, Dr. Sheng Jiang, and Dr. Aiguo Li of 15U1 at SSRF and Dr. Changyong Park at HPCAT, APS, ANL for the technical support on the high-pressure XRD experiment. Gas loading by Sergey N. Tkachev is also acknowledged. HPCAT operations are supported by DOE-NNSA under Award No. DE-NA0001974 and DOE-BES under Award No. DE-FG02-99ER45775, with partial instrumentation funding by NSF. The SXD measurement was conducted at 13BM-C, APS, and ANL. 13BM-C operation is supported by COMPRES through the Partnership for Extreme Crystallography (PX2) project, under NSF Cooperative Agreement EAR-1661511, and by GSECARS under NSF EAR-1634415. The XMCD experiment was conducted at beamline 4ID-D, APS, and ANL. This research used resources from the Advanced Photon Source, a US Department of Energy (DOE) Office of Science User Facility operated for the DOE Office of Science by Argonne National Laboratory under Contract No. DE-AC02-06CH11357.

AUTHOR CONTRIBUTIONS

W.W., J.S., and W.Y. proposed and conceived this project. F.L., D.Z., and W.Y. conducted high-pressure SXD experiments. F.L., G.F., D.H., Y.Z., and W.Y. conducted high-pressure XMCD experiments. Y.H., F.L., W.W., J.Z., L.Y., and W.Y. analyzed the data. J.N. and H.X. performed the DFT calculations. S.C., X.X., and X.L. offer valuable discussion during this project. F.L., Y.H., W.W., W.Y., and J.S. wrote the original version of the manuscript and received feedback from all authors. F.L., Y.H., and J.N. contributed equally to this work.

COMPETING INTERESTS

The authors declare no competing interests.

ADDITIONAL INFORMATION

Supplementary information The online version contains supplementary material available at https://doi.org/10.1038/s41535-022-00522-x.

Correspondence and requests for materials should be addressed to Wenbin Wang, Jian Shen or Wenge Yang.

Reprints and permission information is available at http://www.nature.com/reprints

Publisher's note Springer Nature remains neutral with regard to jurisdictional claims in published maps and institutional affiliations.